Brief Communications

Cell Type-Specific Tuning of Hippocampal Interneuron Firing during Gamma Oscillations *In Vivo*

John J. Tukker,[1] **Pablo Fuentealba,**[1] **Katja Hartwich,**[1,2] **Peter Somogyi,**[1] **and Thomas Klausberger**[1,2]

[1]Medical Research Council Anatomical Neuropharmacology Unit, Oxford University, Oxford OX1 3TH, United Kingdom, and [2]Center for Brain Research, Medical University of Vienna, 1090 Vienna, Austria

Cortical gamma oscillations contribute to cognitive processing and are thought to be supported by perisomatic-innervating GABAergic interneurons. We performed extracellular recordings of identified interneurons in the hippocampal CA1 area of anesthetized rats, revealing that the firing patterns of five distinct interneuron types are differentially correlated to spontaneous gamma oscillations. The firing of bistratified cells, which target dendrites of pyramidal cells coaligned with the glutamatergic input from hippocampal area CA3, is strongly phase locked to field gamma oscillations. Parvalbumin-expressing basket, axo-axonic, and cholecystokinin-expressing interneurons exhibit moderate gamma modulation, whereas the spike timing of distal dendrite-innervating oriens-lacunosum moleculare interneurons is not correlated to field gamma oscillations. Cholecystokinin-expressing interneurons fire earliest in the gamma cycle, a finding that is consistent with their suggested function of thresholding individual pyramidal cells. Furthermore, we show that field gamma amplitude correlates with interneuronal spike-timing precision and firing rate. Overall, our recordings suggest that gamma synchronization *in vivo* is assisted by temporal- and domain-specific GABAergic inputs to pyramidal cells and is initiated in pyramidal cell dendrites in addition to somata and axon initial segments.

Key words: GABAergic interneurons; gamma oscillations; dendrites; hippocampus; juxtacellular recording; synchronization

Introduction

Gamma frequency (30–80 Hz) oscillations are observed in the electroencephalographic signal in a wide range of mammalian brain regions and are correlated with cognitive functions such as working memory, conceptual categorization, and attention (Engel et al., 2001). Furthermore, altered gamma oscillations are seen in brain disorders such as schizophrenia, dementia, and autism (Uhlhaas and Singer, 2006). Many studies have suggested a variety of synaptic and electrical interactions between GABAergic interneurons and/or pyramidal cells as mechanisms for the generation of gamma oscillations (Soltesz and Deschenes, 1993; Hormuzdi et al., 2001; Csicsvari et al., 2003; Traub et al., 2003; Mann et al., 2005; Oren et al., 2006; Vida et al., 2006; Bartos et al., 2007; Fuchs et al., 2007). The suggested involvement of interneurons is supported by the preferential firing of unidentified GABAergic interneurons at particular phases of the extracellular field gamma cycles in behaving and anesthetized rats (i.e., their activity is "gamma modulated") (Bragin et al., 1995; Penttonen et al., 1998;

Csicsvari et al., 2003). Studies on kainate- or carbachol-induced oscillations in brain slices (Hajos et al., 2004; Gloveli et al., 2005; Mann et al., 2005; Oren et al., 2006) and related modeling work (Traub et al., 1996; Bartos et al., 2002) suggest that perisomatic-targeting interneurons, such as basket cells, have a predominant role in generating gamma waves *in vitro*. However, the contribution of many distinct types of GABAergic interneuron to the generation of spontaneous gamma oscillations has not been tested *in vivo*, and their activity in the intact brain is likely to reflect specialized roles in the generation and/or propagation of gamma oscillations.

We report here that the firing patterns of identified interneurons *in vivo* are related to the field gamma oscillations in a cell type-specific manner, suggesting that synchronized gamma oscillations are also initiated in the small oblique and basal dendrites of pyramidal cells.

Materials and Methods

All animal procedures were performed in accordance with the Animals (Scientific Procedures) Act, 1986 (United Kingdom) and associated procedures.

Juxtacellular recordings. After induction of anesthesia with isoflurane, male Sprague Dawley rats (250–350 g) were anesthetized with urethane (1.25 g/kg of body weight, i.p.) and supplemental doses of ketamine and xylazine (20 and 2 mg/kg, respectively) as needed to maintain anesthesia. Extracellular local field potential (LFP) and unit recording were performed with two different glass electrodes (12–30 MΩ) filled with 1.5% Neurobiotin in 0.5 M NaCl. Interneuron action potentials (APs) were counted via thresholding of the on-line filtered (0.8–5 kHz) and digitized (20 kHz) recording; the LFP was filtered on-line (0.3–300 Hz) and digitized at 20 kHz. After unit recording (166–1282 s per recording), the
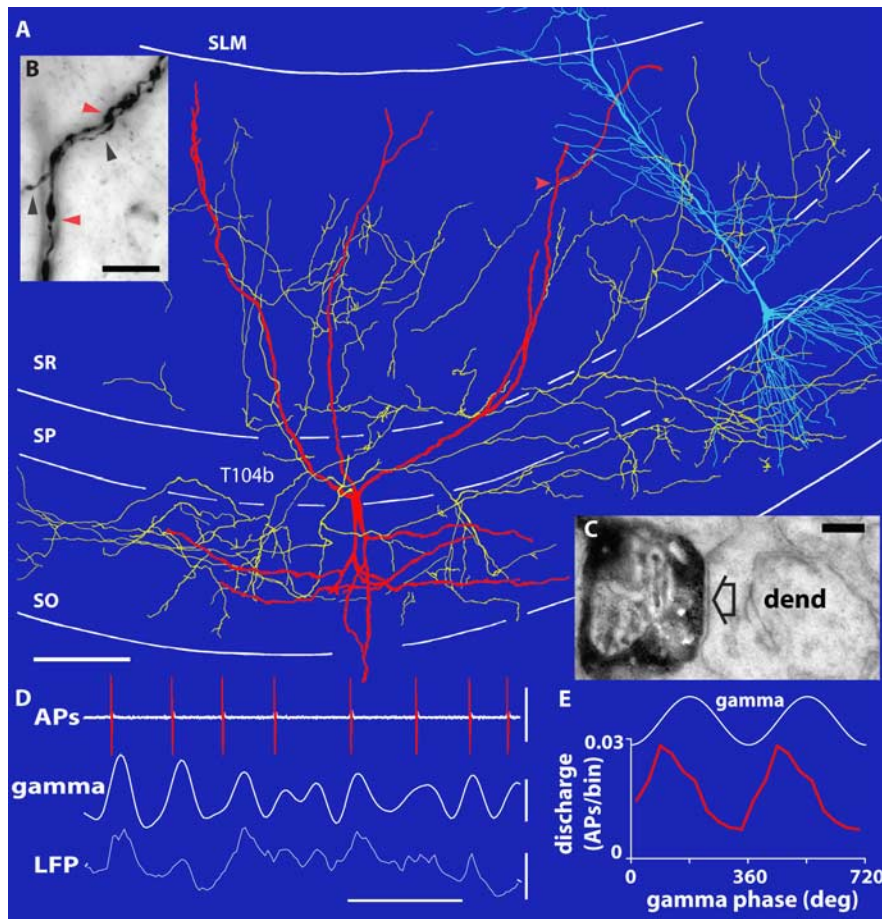
Figure 1. The spike timing of a bistratified interneuron is strongly coupled to the ascending phase of spontaneous gamma oscillations. ***A***, Reconstruction of the Neurobiotin-labeled soma and dendrites (red; shown complete) and axons (yellow; shown from only 5 70-μm-thick sections). A pyramidal cell is superimposed in blue for orientation (different scale and animal). ***B***, Light micrograph of putative dendritic self-innervation sites (red arrow in ***A***). Black and red arrowheads mark axon and dendrite, respectively. ***C***, Electron micrograph showing a terminal of the same bistratified cell (black) making a type 2 synapse (arrow) with an oblique pyramidal dendrite (dend). ***D***, Extracellularly recorded APs (top) and LFPs (bottom; recorded extracellularly with a second electrode in SP) with filtered gamma oscillations (bandpass, 30 – 80 Hz; middle). The bistratified cell fires preferentially at the ascending gamma phase. ***E***, Average discharge rates as a function of gamma phase (per 36° bin; 2 cycles are shown with troughs at 0, 360, and 720°). SO, Stratum oriens. Scale bars: ***A***, 100 μm; ***B***, 10 μm; ***C***, 0.2 μm. Calibration: ***D***, horizontal, 0.05 s; vertical, top, 2 mV; middle and bottom, 0.2 mV.

cystokinin (CCK)-positive cells (T64c, T147a, T152b, T165d, T99d, T123b, and T139c), seven oriens-lacunosum moleculare (O-LM) cells (T64a, T69e, T93b, T95e, T128c, T151b, and T152a), and five bistratified cells (T79e, T83a, T104a, T104b, and C8b). The firing behavior of some of these cells was reported in earlier studies of nongamma rhythmic activity (Klausberger et al., 2003, 2004, 2005).

Analysis of gamma oscillations. Gamma oscillations were detected by digitally filtering (bandpass 30–80 Hz Finite Impulse Response filter; Spike2; Cambridge Electronic Design, Cambridge, UK) the LFP, which did not result in any phase shift, as confirmed by comparing gamma troughs in filtered and raw traces, and selecting those cycles with amplitude greater than the mean cycle amplitude computed over the entire duration of the recording. To prevent AP artifacts influencing gamma oscillations derived from the LFP recording, the LFP and unit APs were always detected in separate electrodes. However, only those data were included in which the coherence of gamma oscillations in the two electrodes could be confirmed during cycles without action potentials. Because gamma oscillations reverse around the stratum pyramidale (SP)-to-stratum radiatum (SR) border, it was crucial to determine in each case the position of the LFP electrode relative to the recorded cell body. This was done by analyzing the following: (1) the relative size/phase of theta and gamma oscillations for the two electrodes; (2) the polarity and size of sharp waves; and (3) stereotactic coordinates. We selected for our analysis only those neurons ($n = 29$ of 70 recorded cells) for which the position of both electrodes could be determined unequivocally. In 25 recordings, the LFP electrode was located in or close to the SP. In four recordings (one PV basket, one axo-axonic, one bistratified, and one CCK-expressing cell), the LFP electrode was located at the SR/lacunosum moleculare (SLM) border. For these recordings, we corrected for the observed gamma phase reversal relative to the LFP from SP (i.e., all reported phase values are relative to SP gamma oscillations).

electrode was advanced toward the cell, and positive current steps were applied to attain juxtacellular Neurobiotin labeling. Spike shape and amplitude were monitored during recording and labeling to ensure that the same cell was recorded and labeled. In addition to interneurons, 15 pyramidal cells were recorded during gamma oscillations; six were confirmed by juxtacellular labeling, and the others were classified according to AP width, complex spike bursts, and firing rate.

Histological analysis. Two to four hours after labeling, cardiac perfusion with saline was followed by ~20 min fixation with 4% paraformaldehyde, 15% v/v saturated picric acid, and 0.05–0.1% glutaraldehyde. Interneuron types were identified using visualization by horseradish peroxidase enzyme reactions (glucose oxidase–diaminobenzidine method) for light and electron microscopy and by the coexpression pattern of molecules demonstrated by immunofluorescence microscopy (Klausberger et al., 2003). Antibodies against parvalbumin (PV) (Mithani et al., 1987) and somatostatin (Vincent et al., 1985) were gifts from Drs. K. Baimbridge and A. Buchan (both from University of British Columbia, Vancouver, British Columbia, Canada), respectively; antibodies against metabotropic glutamate receptor 1α (mGluR1α) (Alvarez et al., 2000) were obtained from DiaSorin (Stillwater, MN). We report here on five axo-axonic cells (T76b, T88a, T103b, T141a, and T151a), five PV-positive basket cells (T75ab, T135b, C3a, P30c, and K3b), seven chole-

To exclude a random effect of LFP electrode location on the depth of modulation or mean gamma phase observed for distinct cell classes, a comparison of the average gamma amplitude for all recordings (overall mean, 0.16 mV; SD, 0.07 mV; $n = 29$) confirmed that there was no systematic difference in gamma amplitude between the recordings for the five cell types [Kruskal–Wallis (KW) test, $\chi^2 = 7.5$; $p = 0.112$; $n = 29$]; excluding the four larger mean gamma amplitudes recorded at the SR/SLM border still did not result in a systematic difference between the gamma amplitudes recorded for different cell types (KW test, $\chi^2 = 6.3$; $p = 0.181$; $n = 25$). Furthermore, we confirmed that the average amplitude of gamma oscillations for each recording was not correlated to the depth of modulation of the simultaneously recorded neuron (two-tailed Spearman's nonparametric correlation test, $r = 0.002$; $p = 0.993$; $n = 29$); considering only recordings of LFP from SP, the correlation was also nonsignificant ($r = -0.186$; $p = 0.372$; $n = 25$), and there were also no significant correlations if tests were performed for cells within a cell class only ($p > 0.5$; $n = 5, 5, 7, 7$ or 5).

Gamma oscillations were further distinguished according to the amplitude of individual cycles: cycle amplitudes >1 SD above the mean were considered "strong gamma," whereas cycle amplitudes 0–1 SD above the mean were classified as "weak gamma"; in all cases, "gamma"

refers to only those cycles with above-mean amplitude. To compare the firing during weak versus strong gamma oscillations for each cell, we used an exact paired Wilcoxon test (StatXact, Cytel, Cambridge, MA).

For each AP time point t_n, for which the coincident gamma oscillation cycle displayed the correct period (12.5–33.3 ms) and amplitude (see above), the phase was computed using the preceding (t_i) and following (t_{i+1}) gamma trough times (phase = $[(t_n - t_i)/(t_{i+1} - t_i)] \times 360°$). Firing was regarded as gamma modulated if the Rayleigh test indicated that spike-time phases (relative to the detected gamma oscillations) were not distributed uniformly around the gamma cycle ($p < 0.05$) (Zar, 1999). For each cell, we quantified the depth of modulation by summing all spike-time phases as unity vectors; the resulting vector sum was normalized by the number of spikes (Zar, 1999). Depending on the orientations of the different phase angles, the length of the normalized vector ("r") can range from 0 (uniform distribution) to 1 (all phase angles identical). The direction of r indicates the cell's mean phase angle. To test whether mean phase angles were uniformly distributed, we applied the Moore test (Zar, 1999).

Phase histograms (36° bins) represent AP timing relative to the gamma oscillation troughs in SP. Discharge rate in the phase histograms was computed by dividing the number of detected APs per bin by the number of detected gamma cycles. Spike2 software (Cambridge Electronic Design) was used for all recordings and for the analysis described above. Depth of modulation was compared in cells of different types using both two-sample and multisample exact KW tests (StatXact, Cytel).

To compare preferred gamma phase angles for CB1-positive versus CB1-negative interneuron classes, for each class we summed the vectors representing all cells belonging to that class and calculated the angular difference between the two vector sums. To evaluate significance, we used a two-sample permutation test (Good, 2000) implemented in MATLAB (The MathWorks, Natick, MA): all instances of the two cell groups were randomly divided into two sets, and the angular difference was computed for all possible permutations; by comparing the angular difference between the original groups with the distribution of all possible angular differences, an exact p value was computed. The statistical software package StatXact (Cytel) uses similar methods for exact KW and Wilcoxon statistics. We selected these tests because they make no assumptions about distributions and because of their suitability for small sample sizes. Only test results with $p < 0.05$ are reported here. To control the type 1 error caused by multiple testing, adapted criterion p values were computed based on false discovery rate control (Benjamini and Hochberg, 1995), which is more powerful than the standard Bonferroni correction.

Results

We performed extracellular recordings of interneurons in the hippocampal CA1 area of anesthetized rats during spontaneously occurring gamma oscillations (mean ± SD, 43 ± 2 Hz; $n = 29$) recorded from a second electrode (see Materials and Methods). Gamma oscillations occurred nested onto slower (4–8 Hz) theta oscillations (Bragin et al., 1995; Penttonen et al., 1998) and also during nontheta b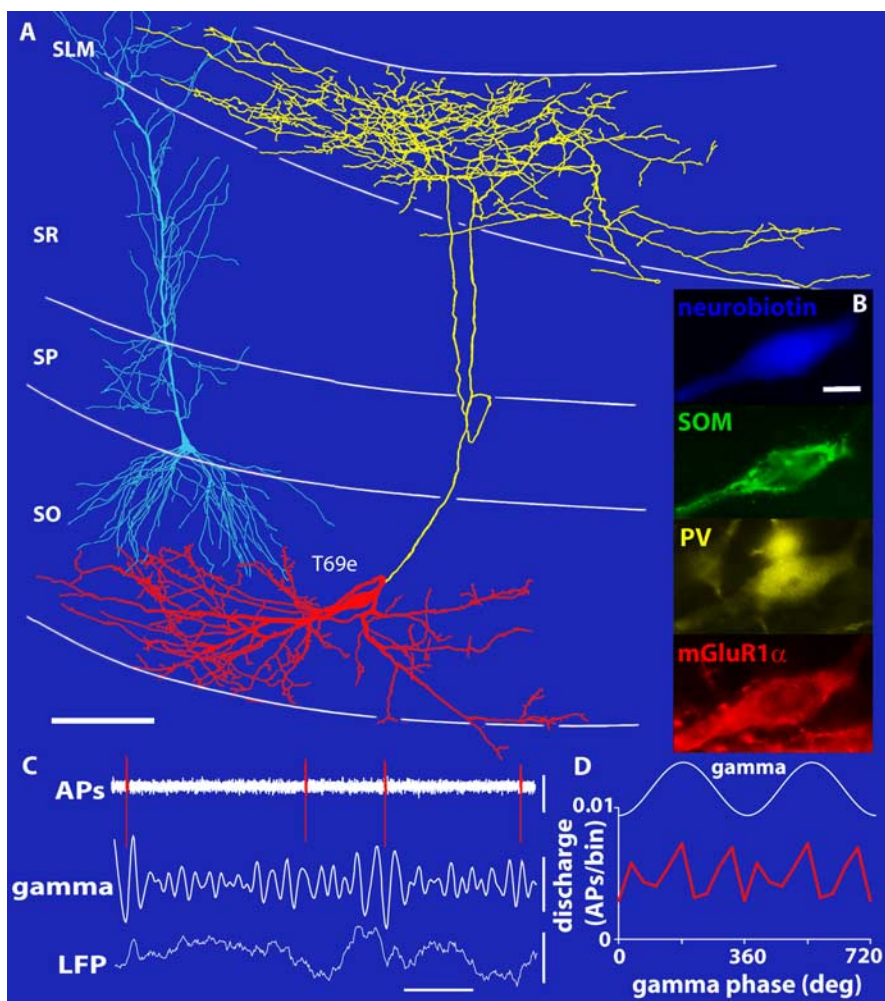rain states (Csicsvari et al., 2003). All data were pooled, because no differences in gamma-related firing patterns of single cells were observed in the two network states (data not shown), as described previously in behaving rats (Csicsvari et al., 2003). Recorded interneurons were individually labeled with the juxtacellular filling method and unequivocally classified by their expression of neurochemical markers, dendritic and axonal arborizations, and electron microscopic identification of postsynaptic targets (Klausberger et al., 2003) (Figs. 1, 2). Our analysis revealed a significant modulation of spike timing during gamma oscillations (criterion: Rayleigh test, $p < 0.05$) for all recorded axo-axonic ($n = 5$), PV-expressing basket ($n = 5$), and bistratified ($n = 5$) (Fig. 1) cells and five of seven CCK-expressing cells, but only two of seven identified O-LM cells (Figs. 2, 3A).

To quantify the depth of gamma modulation (Figs. 1D,E, 2C,D), we computed a normalized vector sum of the gamma phase angles of all spike times for each cell (Fig. 3A) (see Materials and Methods), where the vector length and angle represent depth of modulation and preferred phase, respectively. Seven of 15 CA1 pyramidal cells showed significant gamma modulation with a depth of modulation comparable with interneurons (median, 0.14; range,

Figure 2. Spike timing of an O-LM cell is not coupled to field gamma oscillations. **A**, Reconstructions of the Neurobiotin-labeled soma and dendrites (red; shown complete) and axons (yellow; shown from only 12 70-μm-thick sections). **B**, The Neurobiotin-labeled O-LM cell is immunopositive for PV, somatostatin (SOM), and mGluR1α. **C**, Extracellularly recorded APs (top) and LFPs (bottom; recorded extracellularly with a second electrode in SP) with filtered gamma oscillations (bandpass, 30 – 80 Hz; middle). The O-LM cell firing is not coupled to any particular gamma phase. **D**, Average discharge rates as a function of gamma phase (per 36° bin; 2 cycles are shown). SO, Stratum oriens. Scale bars: **A**, 100 μm; **B**, 10 μm. Calibration: **C**, horizontal, 0.1 s; vertical, top, 0.2 mV; middle, 0.1 mV; bottom, 0.4 mV.
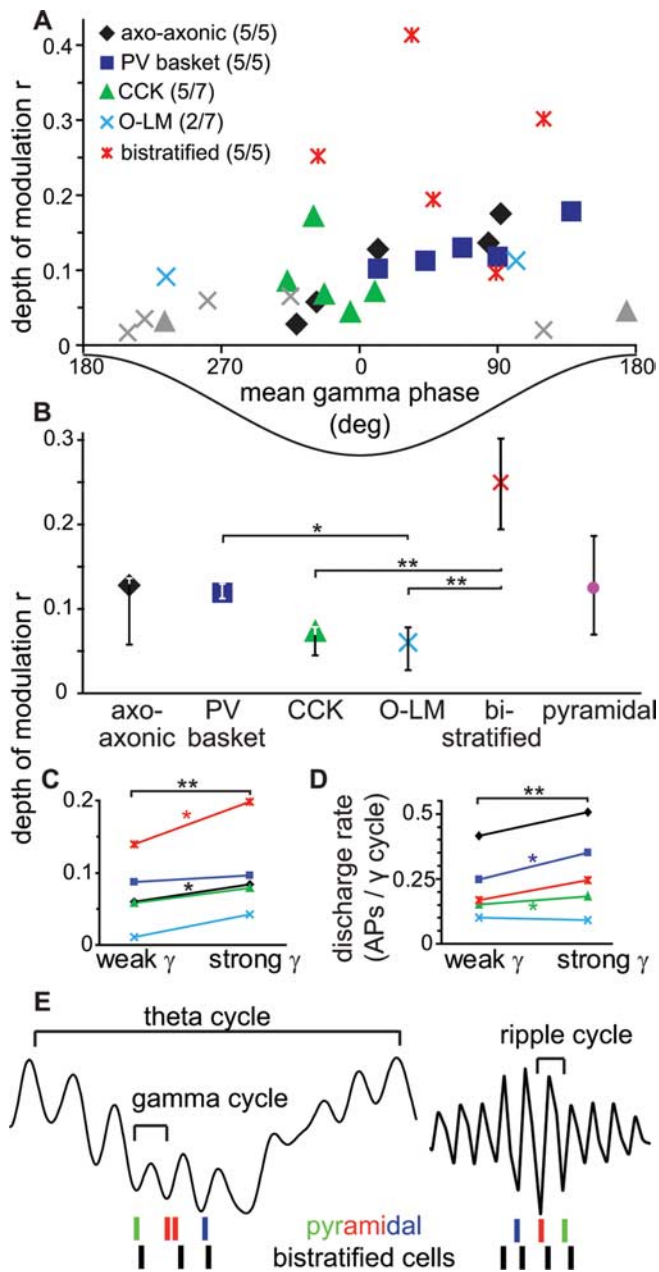
Figure 3. Discharge of distinct interneuron classes is differentially modulated during field gamma oscillations. **A**, Gamma-modulated firing of interneurons characterized by the depth of modulation, r, and the mean preferred gamma phase angle for each identified cell ($n = 29$). Different symbols mark different cell types as indicated; for each cell type, numbers in parentheses indicate the number of significantly modulated cells (Rayleigh test, $p < 0.05$)/total number of cells per cell class. Gray symbols represent cells not modulated by gamma. The trough and peak of the field gamma cycle in SP are at 0 and 180°, respectively. **B**, Bistratified cell firing was more strongly gamma modulated than O-LM and CCK cell firing; PV basket cell firing was also more strongly gamma modulated than O-LM cell firing. Median and interquartile range of all cells are shown, including cells not significantly modulated. **$p < 0.01$; *$p < 0.02$ (exact KW test). **C**, **D**, Interneurons show significantly stronger phase coupling (**C**) and higher discharge rates (**D**) during strong gamma cycles with high field gamma amplitude than during weak gamma cycles with lower amplitude. *$p < 0.05$; **$p < 0.001$ (paired one-tailed Wilcoxon signed-rank test). **E**, Schematic spike timing of sequentially active pyramidal place cells (colored spikes) during theta-nested gamma oscillations and their reverse and compressed replay during subsequent ripple oscillations (Buzsaki, 1989; Foster and Wilson, 2006). Pyramidal cells fire at the trough and ascending phase of gamma and ripple oscillations, with similar phase relation relative to bistratified cells (black spikes).

0.07–0.40; $n = 7$). The depth of modulation of interneurons revealed a significant difference between different classes ($p = 0.001$, two-tailed multisample exact KW test; $n = 29$) (Fig. 3B).

Surprisingly, bistratified cells (Fig. 1), which, together with glutamatergic input from the CA3 area, target the oblique dendrites of pyramidal cells (Klausberger et al., 2004), showed the strongest gamma modulation (median $r = 0.252$; interquartile range, 0.194–0.302; $n = 5$) (Fig. 3B). This gamma-modulated GABAergic input might explain the gamma-frequency membrane oscillations observed in pyramidal cell dendrites (Penttonen et al., 1998) and could provide a temporal frame in SR for the recently discovered dendritic branch-specific spiking activity of CA1 pyramidal cells (Losonczy and Magee, 2006). Such a firing pattern in bistratified cells could be promoted by the gamma oscillation-generating CA3 input (Csicsvari et al., 2003) and supported by autaptic innervation (Bacci and Huguenard, 2006) (Fig. 1B) and gap-junctional coupling (Baude et al., 2007). In contrast, the spike timing of O-LM cells (Fig. 2) exhibited no or very little modulation during gamma oscillations (median $r = 0.059$; interquartile range, 0.028–0.078; $n = 7$) (Fig. 3B), different from bistratified cells ($p = 0.005$; two-tailed exact KW test; $n = 12$). Axons of O-LM cells innervate the most distal pyramidal cell dendrites, which receive glutamatergic input from the entorhinal cortex transmitting spatial information from grid cells (Hafting et al., 2005). In slice preparations of the CA3 area, the spike timing of O-LM cells was modulated by carbachol-induced gamma oscillations (Hajos et al., 2004), although their firing rates were limited to theta frequencies (Gloveli et al., 2005). Our results suggest that, in the CA1 area, O-LM cells do not contribute to the generation of gamma oscillations in anesthetized rats.

Axo-axonic, PV basket, and CCK-expressing cells showed moderate or weak gamma modulation (Fig. 3B). However, because of the high concentration of their GABAergic synapses in the pyramidal cell body layer, perisomatic-targeting interneurons might nonetheless contribute significantly to the generation of field gamma oscillations, as reported for *in vitro* preparations (Mann et al., 2005; Oren et al., 2006; Vida et al., 2006).

Under our conditions, most interneurons fired preferentially at or after the troughs of extracellular gamma oscillations in SP ($p < 0.001$, multisample Moore test; $n = 29$) (Fig. 3A), like nonidentified interneurons in behaving rats (Csicsvari et al., 2003). Interestingly, the five significantly modulated CCK-expressing interneurons, which express cannabinoid CB1 receptors along their axons, fired earlier than the other gamma-modulated cells ($p = 0.004$, two-sample permutation test; $n = 22$). Seven gamma-modulated pyramidal cells fired at the trough or rising phase of gamma oscillations in SP (range, 328°-164°), a finding that is consistent with recordings from behaving animals (Csicsvari et al., 2003). Thus, inhibition from CCK-expressing interneurons could be well timed to set a threshold for the firing of CA1 pyramidal cells: pyramidal cells that overcome the inhibitory threshold could subsequently reduce the inhibition from CCK-expressing GABAergic cells by releasing endocannabinoids and activating CB1 receptors on the terminals of their afferent GABAergic synapses (Katona et al., 1999; Wilson and Nicoll, 2001). The reduction of GABA release specifically to firing cells might further enhance the contrast between spiking and silent pyramidal cells and support sparse coding in the hippocampus.

The amplitude of extracellular gamma oscillations varied considerably, as reported for behaving rats (Csicsvari et al., 2003). If synchronously firing interneurons contribute to the generation of these oscillations, one might expect a correlation between gamma oscillation amplitude and interneuron firing (Bragin et

al., 1995). Indeed, interneurons as a population significantly increased the depth of their gamma-modulation tuning (Fig. 3C) and firing rate (Fig. 3D) during strong as opposed to weak gamma oscillations (see Materials and Methods). These data demonstrate a correlation between the magnitude of gamma oscillations in the extracellular field potential and the firing patterns of GABAergic interneurons, suggesting a causal relationship.

Discussion

We have shown a cell type-specific tuning of hippocampal interneuron firing during gamma oscillations, a finding that suggests a division of labor between distinct interneuron types. The lack of phase locking of O-LM cell firing indicates that these cells do not contribute to the synchronization of distal pyramidal cell dendrites to field gamma oscillations. The gamma-modulated firing of CCK-expressing interneurons at an early gamma phase, before pyramidal cells fire (Csicsvari et al., 2003), together with their CB1 receptor expression, could contribute to setting dynamic, activity-dependent thresholds for pyramidal cells. Axo-axonic and PV basket cells exhibit moderate but significant gamma modulation. During hippocampal theta oscillations, associated with active "exploratory" behavior (Vanderwolf, 1969), these cells fire preferentially on the peak or descending phase recorded from CA1 stratum pyramidale (Klausberger et al., 2003). Interestingly, gamma oscillations occur during theta oscillations with highest amplitude also at the extracellular CA1 theta peaks (Penttonen et al., 1998). This coincidence together with their dense GABAergic innervation in the pyramidal cell layer suggests that PV basket and axo-axonic cells play a major role in the generation of field gamma oscillations. However, these cells might not gamma modulate the spiking of pyramidal cells, which fire preferentially around the theta troughs together with bistratified interneurons (O'Keefe, 1976; Klausberger et al., 2004). Thus, during theta oscillations, strongly gamma-modulated firing of bistratified cells provides GABAergic input with gamma rhythmicity to pyramidal cells coding for space (O'Keefe, 1976). Bistratified cells could generate precise windows of excitability in the innervated dendritic branches of single pyramidal cells (Pouille and Scanziani, 2004). By synchronizing branches of many pyramidal cells, bistratified cells can phase excitatory input from the CA3 area to the population gamma phase on time scales consistent with spike timing-dependent plasticity (Markram et al., 1997).

Bistratified cells are also very active during sharp wave-associated ripples (120–200 Hz) (Klausberger et al., 2004) and might have a similar spike-timing relationship with simultaneously active pyramidal cells (Csicsvari et al., 2003) during both gamma and ripple oscillations (Fig. 3E). Therefore, bistratified cells could contribute to the temporal compression of pyramidal cell assembly firing that occurs between theta-nested gamma oscillations during active behavior and memory consolidation during sharp wave-associated ripples (Buzsaki, 1989; Foster and Wilson, 2006).

References

Alvarez FJ, Villalba RM, Carr PA, Grandes P, Somohano PM (2000) Differential distribution of metabotropic glutamate receptors 1a, 1b, and 5 in the rat spinal cord. J Comp Neurol 422:464–487.

Bacci A, Huguenard JR (2006) Enhancement of spike-timing precision by autaptic transmission in neocortical inhibitory interneurons. Neuron 49:119–130.

Bartos M, Vida I, Frotscher M, Meyer A, Monyer H, Geiger JR, Jonas P (2002) Fast synaptic inhibition promotes synchronized gamma oscillations in hippocampal interneuron networks. Proc Natl Acad Sci USA 99:13222–13227.

Bartos M, Vida I, Jonas P (2007) Synaptic mechanisms of synchronized gamma oscillations in inhibitory interneuron networks. Nat Rev Neurosci 8:45–56.

Baude A, Bleasdale C, Dalezios Y, Somogyi P, Klausberger T (2007) Immunoreactivity for the GABAA receptor α1 subunit, somatostatin and connexin36 distinguishes axoaxonic, basket, and bistratified interneurons of the rat hippocampus. Cereb Cortex, in press.

Benjamini Y, Hochberg Y (1995) Controlling for the false discovery rate: a practical and powerful approach to multiple testing. J R Stat Soc B 57:289–300.

Bragin A, Jando G, Nadasdy Z, Hetke J, Wise K, Buzsaki G (1995) Gamma (40–100 Hz) oscillation in the hippocampus of the behaving rat. J Neurosci 15:47–60.

Buzsaki G (1989) Two-stage model of memory trace formation: a role for "noisy" brain states. Neuroscience 31:551–570.

Csicsvari J, Jamieson B, Wise KD, Buzsaki G (2003) Mechanisms of gamma oscillations in the hippocampus of the behaving rat. Neuron 37:311–322.

Engel AK, Fries P, Singer W (2001) Dynamic predictions: oscillations and synchrony in top-down processing. Nat Rev Neurosci 2:704–716.

Foster DJ, Wilson MA (2006) Reverse replay of behavioural sequences in hippocampal place cells during the awake state. Nature 440:680–683.

Fuchs EC, Zivkovic AR, Cunningham MO, Middleton S, Lebeau FE, Bannerman DM, Rozov A, Whittington MA, Traub RD, Rawlins JN, Monyer H (2007) Recruitment of parvalbumin-positive interneurons determines hippocampal function and associated behavior. Neuron 53:591–604.

Gloveli T, Dugladze T, Saha S, Monyer H, Heinemann U, Traub RD, Whittington MA, Buhl EH (2005) Differential involvement of oriens/pyramidale interneurones in hippocampal network oscillations in vitro. J Physiol (Lond) 562:131–147.

Good P (2000) Permutation tests: a practical guide to resampling methods for testing hypotheses, Ed 2. New York: Springer.

Hafting T, Fyhn M, Molden S, Moser MB, Moser EI (2005) Microstructure of a spatial map in the entorhinal cortex. Nature 436:801–806.

Hajos N, Palhalmi J, Mann EO, Nemeth B, Paulsen O, Freund TF (2004) Spike timing of distinct types of GABAergic interneuron during hippocampal gamma oscillations in vitro. J Neurosci 24:9127–9137.

Hormuzdi SG, Pais I, LeBeau FE, Towers SK, Rozov A, Buhl EH, Whittington MA, Monyer H (2001) Impaired electrical signaling disrupts gamma frequency oscillations in connexin 36-deficient mice. Neuron 31:487–495.

Katona I, Sperlagh B, Sik A, Kafalvi A, Vizi ES, Mackie K, Freund TF (1999) Presynaptically located CB1 cannabinoid receptors regulate GABA release from axon terminals of specific hippocampal interneurons. J Neurosci 19:4544–4558.

Klausberger T, Magill PJ, Marton LF, Roberts JD, Cobden PM, Buzsaki G, Somogyi P (2003) Brain-state- and cell-type-specific firing of hippocampal interneurons in vivo. Nature 421:844–848.

Klausberger T, Marton LF, Baude A, Roberts JD, Magill PJ, Somogyi P (2004) Spike timing of dendrite-targeting bistratified cells during hippocampal network oscillations in vivo. Nat Neurosci 7:41–47.

Klausberger T, Marton LF, O'Neill J, Huck JH, Dalezios Y, Fuentealba P, Suen WY, Papp E, Kaneko T, Watanabe M, Csicsvari J, Somogyi P (2005) Complementary roles of cholecystokinin- and parvalbumin-expressing GABAergic neurons in hippocampal network oscillations. J Neurosci 25:9782–9793.

Losonczy A, Magee JC (2006) Integrative properties of radial oblique dendrites in hippocampal CA1 pyramidal neurons. Neuron 50:291–307.

Mann EO, Suckling JM, Hajos N, Greenfield SA, Paulsen O (2005) Perisomatic feedback inhibition underlies cholinergically induced fast network oscillations in the rat hippocampus in vitro. Neuron 45:105–117.

Markram H, Lubke J, Frotscher M, Sakmann B (1997) Regulation of synaptic efficacy by coincidence of postsynaptic APs and EPSPs. Science 275:213–215.

Mithani S, Atmadja S, Baimbridge KG, Fibiger HC (1987) Neuroleptic-induced oral dyskinesias: effects of progabide and lack of correlation with regional changes in glutamic acid decarboxylase and choline acetyltransferase activities. Psychopharmacology (Berl) 93:94–100.

O'Keefe J (1976) Place units in the hippocampus of the freely moving rat. Exp Neurol 51:78–109.

Oren I, Mann EO, Paulsen O, Hajos N (2006) Synaptic currents in anatom-

ically identified CA3 neurons during hippocampal gamma oscillations *in vitro*. J Neurosci 26:9923–9934.

Penttonen M, Kamondi A, Acsady L, Buzsaki G (1998) Gamma frequency oscillation in the hippocampus of the rat: intracellular analysis in vivo. Eur J Neurosci 10:718–728.

Pouille F, Scanziani M (2004) Routing of spike series by dynamic circuits in the hippocampus. Nature 429:717–723.

Soltesz I, Deschenes M (1993) Low- and high-frequency membrane potential oscillations during theta activity in CA1 and CA3 pyramidal neurons of the cat hippocampus under ketamine-xylazine anesthesia. J Neurophysiol 70:97–116.

Traub RD, Whittington MA, Colling SB, Buzsaki G, Jefferys JG (1996) Analysis of gamma rhythms in the rat hippocampus in vitro and in vivo. J Physiol (Lond) 493:471–484.

Traub RD, Pais IE, Bibbig A, LeBeau FE, Buhl EH, Hormuzdi SG, Monyer H, Whittington MA (2003) Contrasting roles of axonal (pyramidal cell) and dendritic (interneuron) electrical coupling in the generation of neuronal network oscillations. Proc Natl Acad Sci USA 100:1370–1374.

Uhlhaas PJ, Singer W (2006) Neural synchrony in brain disorders: relevance for cognitive dysfunctions and pathophysiology. Neuron 52:155–168.

Vanderwolf CH (1969) Hippocampal electrical activity and voluntary movement in the rat. Electroencephalogr Clin Neurophysiol 26:407–418.

Vida I, Bartos M, Jonas P (2006) Shunting inhibition improves robustness of gamma oscillations in hippocampal interneuron networks by homogenizing firing rates. Neuron 49:107–117.

Vincent SR, McIntosh CH, Buchan AM, Brown JC (1985) Central somatostatin systems revealed with monoclonal antibodies. J Comp Neurol 238:169–186.

Wilson RI, Nicoll RA (2001) Endogenous cannabinoids mediate retrograde signalling at hippocampal synapses. Nature 410:588–592.

Zar JH (1999) Biostatistical analysis, Ed 4. Upper Saddle River, NJ: Prentice Hall.